



## OPEN ACCESS

## EDITED BY

Alessandro Retino,  
UMR7648 Laboratoire de physique des  
plasmas (LPP), France

## REVIEWED BY

Octav Marghitu,  
Space Science Institute, Romania  
Xiao-Jia Zhang,  
University of California, Los Angeles,  
United States

## \*CORRESPONDENCE

Joseph E. Borovsky,  
jborovsky@spascescience.org

## SPECIALTY SECTION

This article was submitted  
to Space Physics,  
a section of the journal  
Frontiers in Astronomy and Space  
Sciences

RECEIVED 14 May 2022

ACCEPTED 29 August 2022

PUBLISHED 26 September 2022

## CITATION

Borovsky JE (2022), Loss-cone-shift  
maps for the Earth's magnetosphere.  
*Front. Astron. Space Sci.* 9:944169.  
doi: 10.3389/fspas.2022.944169

## COPYRIGHT

© 2022 Borovsky. This is an open-  
access article distributed under the  
terms of the [Creative Commons  
Attribution License \(CC BY\)](https://creativecommons.org/licenses/by/4.0/). The use,  
distribution or reproduction in other  
forums is permitted, provided the  
original author(s) and the copyright  
owner(s) are credited and that the  
original publication in this journal is  
cited, in accordance with accepted  
academic practice. No use, distribution  
or reproduction is permitted which does  
not comply with these terms.

# Loss-cone-shift maps for the Earth's magnetosphere

Joseph E. Borovsky\*

Center for Space Plasma Physics, Space Science Institute, Boulder, CO, United States

Because of finite-gyroradii effects, the atmospheric loss cone for energetic particles in the magnetosphere is shifted away from the magnetic-field direction. Using the Tsyganenko T96 magnetic-field model, maps of the magnitude of the angular shift of the loss cone are created for electrons, protons, and singly-ionized oxygen in the nightside magnetosphere. When the shift exceeds about 5°–10°, stochastic scattering of particles occurs. For protons and oxygen, this loss-cone shift is quite large, even in the dipolar portions of the magnetosphere, and stochastic scattering of protons and oxygen can occur in those regions. Hence, the ring-current ion population probably exhibits a robustly shifted loss cone and stochastic scattering in the dipole magnetosphere. For electrons, large loss-cone shifts and stochastic scattering are restricted to the magnetotail near and beyond the transition region.

## KEYWORDS

magnetospheres, pitch-angle scattering, particle orbits, radiation belts, field-linecurvature scattering

## Introduction

Owing to finite-gyroradius effects the center of the atmospheric loss cone in the Earth's magnetosphere shifts away from the direction of the magnetic-field line (Mozer, 1966; Il'in et al., 1992; Il'ina et al., 1993; Porazik et al., 2014; Sanchez et al., 2019; Powis et al., 2019; Willard et al., 2019; Borovsky et al., 2022a,b). For positive ions the angular shift of both the northern and southern loss cones is westward and for electrons the angular shift of both loss cones is eastward. Because of the shift the northern and southern loss cones are no longer 180° apart. This angular shift  $\theta_{\text{shift}}$  is most-easily calculated *via* the “Mozer transform” (Mozer, 1966; Borovsky et al., 2020a,b, 2022a,b)

$$\theta_{\text{shift}} = \arcsin(V_{\text{curve}}/V) \quad (1)$$

where  $v$  is the total velocity of the particle and  $v_{\text{curve}}$  is the curvature-drift velocity of that particle

$$\mathbf{v}_{\text{curve}} = (m\gamma c/qB^3)v_{\parallel}^2(\mathbf{B} \times \nabla B) \quad (2)$$

(e.g. Eq. 2.17 of Roederer and Zhang (2014)), where  $m$  is the mass of the particle,  $q$  the signed charge of the particle,  $c$  the speed of light,  $v_{\parallel}$  is the component of the particle's velocity that is parallel to the magnetic field, and  $\gamma = (1 - (v^2/c^2))^{-1/2}$  is the particle's relativistic factor.

It can be important for a number of reasons to understand and assess this loss-cone shift away from the magnetic-field direction. (1) Particle orbits in the magnetosphere are organized by the shift away from the magnetic-field direction whereas particle scattering by plasma waves is organized by the magnetic-field direction (e.g. Borovsky et al., 2022a). (2) The empty-loss-cone distribution of particles is shifted away from the magnetic-field direction, perhaps creating plasma-wave instabilities (e.g. Borovsky et al., 2022a). (3) Experiments that need to critically know where the atmospheric loss cone is (e.g. Porazik et al., 2014; Sanchez et al., 2019; Willard et al., 2019; Borovsky et al., 2020a,b) need to account for this angular loss-cone shift. (4) The magnitude of the loss-cone angular shift is directly related to whether or not there will be field-line-curvature scattering of the particles (e.g. Il'in et al., 1992; Il'ina et al., 1993; Borovsky et al., 2022a,b).

In a dipole magnetic-field geometry the loss-cone angular shift can be algebraically calculated (e.g. Borovsky et al., 2022a,b). In the real distorted-field magnetosphere the angular shift is not known. However, using a mathematical magnetic-field model for the magnetosphere the loss-cone shifts can be numerically estimated.

In this report, maps of the value of  $\theta_{\text{shift}}$  in the noon-midnight meridional plane are created and examined for electrons, protons, and oxygen ions using the T96 (Tsyganenko, 1995; Tsyganenko and Stern, 1996) magnetic-field model to calculate the magnetic-field strength  $B$  and the local  $(\mathbf{B} \times \nabla B)$  curvature of the magnetic-field lines. The noon-midnight meridian maps are applicable to the Canadian longitude when Canada is at local midnight near the winter solstice: hence the dipole will have a very strong tilt away from the Sun-Earth line. At this time the Earth's spin axis is tilted away from the Sun by  $23^\circ$  and the dipole is tilted a further  $11^\circ$ . Maps in the equatorial plane in the absence of dipole tilt are also created and examined. The parameters used for the T96 model were  $B_z = -5$  nT for the solar wind and  $Dst = -30$  nT.

## The shift maps

Figure 1 plots the half-angle  $\theta_{\text{L.C.}}$  of the atmospheric loss cone (colors) in the noon-midnight meridian of the nightside magnetosphere calculated using the tilted dipole T96 field. In the plot  $Z$  is the north-south direction and  $X$  is the Sun-Earth direction in GSE coordinates. Magnetic-field lines are drawn in black. The purple dashed line denotes the  $23^\circ$  tilted equatorial plane of the Earth.

Figure 2 shows maps of the magnitude of the loss-cone angular shift eastward in the nightside magnetosphere for electrons of 50 keV (top panel) and 1 MeV (bottom panel). Magnetic-field lines are drawn in black and the Earth's tilted equatorial plane is denoted by the purple dashed curve. Note that there is a strong "dipole tilt" the with the dipole equator (not

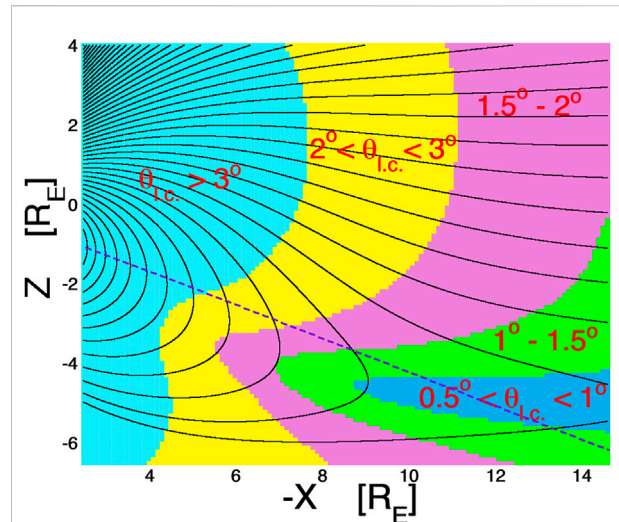
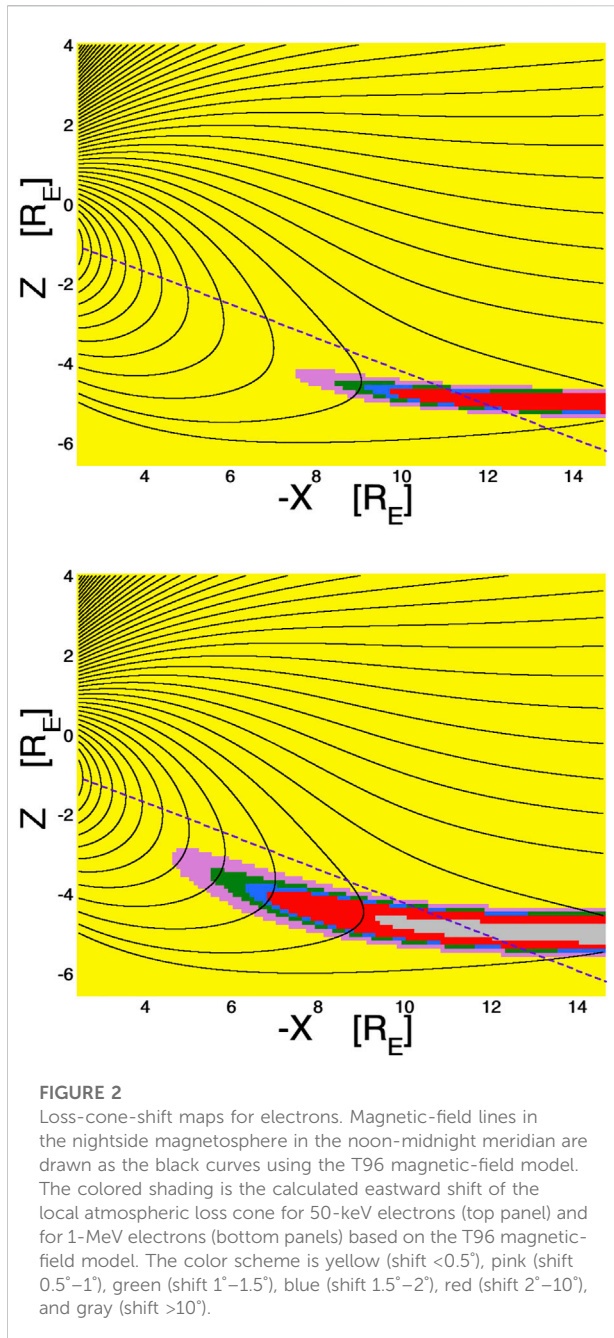


FIGURE 1

The half-angle of the atmospheric loss cone  $\theta_{\text{L.C.}}$  is plotted in color. In the light-blue shaded region  $\theta_{\text{L.C.}} > 3^\circ$ , in the yellow region  $2^\circ < \theta_{\text{L.C.}} < 3^\circ$ , in the pink shaded region  $1.5^\circ < \theta_{\text{L.C.}} < 2^\circ$ , in the green shaded region  $1^\circ < \theta_{\text{L.C.}} < 1.5^\circ$ , and in the blue shaded region  $0.5^\circ < \theta_{\text{L.C.}} < 1^\circ$ .

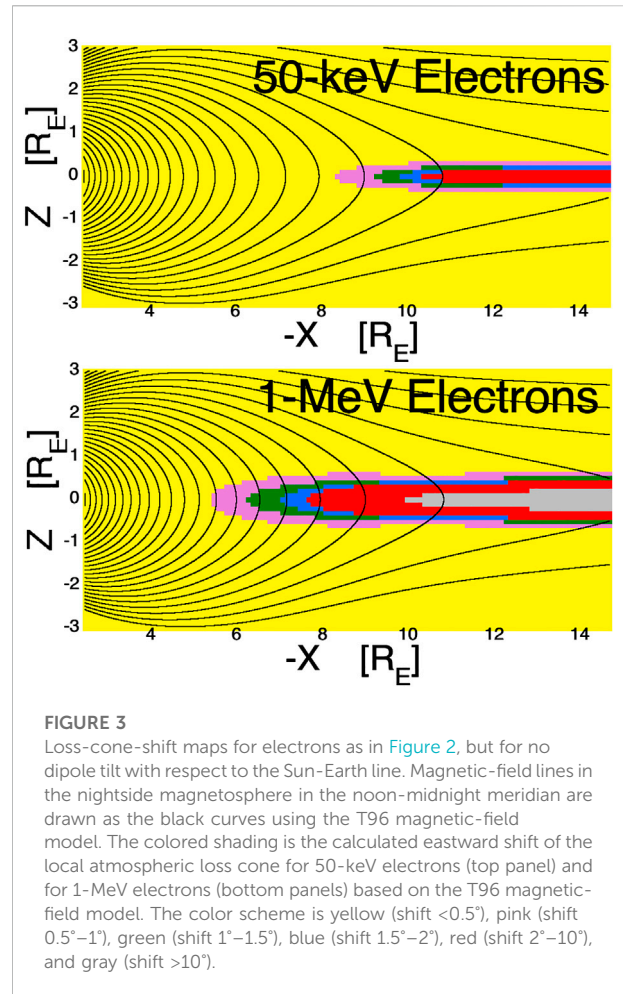
marked) southward from the geographic equator on the nightside. The yellow-shaded zones in Figure 2 are regions of the magnetosphere where the atmospheric loss cone angular shift  $\theta_{\text{shift}}$  is small ( $< 0.5^\circ$ ) and the other colors denote regions where the shift  $\theta_{\text{shift}}$  is stronger (see Figure caption). Comparing the two panels (of Figure 2) it is seen that the shift is larger for 1-MeV electrons than it is for 50-keV electrons: this is because the 1-MeV electrons have larger gyroradii than do the 50-keV electrons. Note in both panels that the loss-cone shift is large where the curvature of the field lines is strong. If anywhere along a field line there is a loss-cone shift  $\theta_{\text{shift}} > 10^\circ$ , particles on that field line will undergo field-line-curvature (FLC) scattering (Borovsky et al., 2022a,b) and their orbits will become stochastic. This is because FLC scattering is parameterized by an "adiabaticity parameter"  $\epsilon = r_{\text{gyro}}/R_c$  (Il'in et al., 1992; Il'ina et al., 1993), where  $r_{\text{gyro}}$  is the gyroradius of the particle with pitch angle  $90^\circ$  and  $R_c$  is the field-line radius of curvature:  $\epsilon = r_{\text{gyro}}/R_c = 3\gamma m c v_o/eB$  is related to the loss-cone shift at the equator  $\theta_{\text{shift}} = \arcsin(3\gamma m c v_o/eB)$ , where at small pitch angles  $\epsilon \approx \theta_{\text{shift}}$  where  $\theta_{\text{shift}}$  is measured in radians (cf. Borovsky et al., 2022a). Stochastic behavior onsets when  $\epsilon \sim 0.1-0.2$  (Birmingham, 1984; Chirikov, 1987; Il'ina et al., 1993), which corresponds to  $\theta_{\text{shift}} \sim 5.7^\circ-11.5^\circ$ . Note that as  $\epsilon$  and  $\theta_{\text{shift}}$  increase, the onset to stochasticity is slow, not abrupt at particular values of  $\epsilon$  and  $\theta_{\text{shift}}$  (cf. Figure 5 of Borovsky et al., 2022a or Figure 6 of Borovsky et al., 2022b).

During other times of the year (away from the December solstice wherein the dipole tilt from the Sun-Earth line is strong) the picture in the nightside magnetosphere is very similar to that



depicted in Figure 2. This is demonstrated in Figure 3 where the maps of Figure 2 are recalculated from the T96 model with no dipole tilt with respect to the Sun-Earth line. Again, the largest angular shift of the loss cone occurs in the midplane of the plasma sheet where the field-line curvature is strongest.

In Figure 4 two westward-angular-shift maps for protons in the nightside magnetosphere are shown: the top panel is for 10-keV protons (energies typical of the ion plasma sheet) and the bottom panel is for 200-keV protons (energies typical of substorm-injected ions). The gyroradii of protons are in



general much greater than the gyroradii of electrons and so the magnitude of the angular shift  $\theta_{\text{shift}}$  of the loss cone tends to be greater for protons than for electrons. With the loss cone typically being in the range of  $3^\circ$  or less (cf. Figure 1), one could consider the angular shift of the loss cone to be “significant” if it is  $2^\circ$  or more. The maps of Figure 4 indicate that the angular shift of the loss cone can be significant ( $\theta_{\text{shift}} > 2^\circ$ , red shading) for 200-keV protons at  $L = 4$  and the loss-cone shift can be significant for 10-keV protons at  $L = 6$ . The gray shading ( $\theta_{\text{shift}} > 10^\circ$ ) in the two panels of Figure 4 indicates that one can expect 10-keV protons to have stochastic orbits at  $L = 8$  and 200-keV protons to have stochastic orbits at  $L = 5$  owing to field-line-curvature scattering.

Figure 5 shows two westward-angular-shift maps for oxygen  $\text{O}^+$  in the nightside magnetosphere: the top panel is for 10-keV oxygen (energies typical of the ion plasma sheet) and the bottom panel is for 200-keV oxygen (energies typical of substorm-injected ions). The gyroradii of  $\text{O}^+$  is 4 times the gyroradii of protons at the same kinetic energy and so the angular shift  $\theta_{\text{shift}}$  of the loss cone tends to be greater for

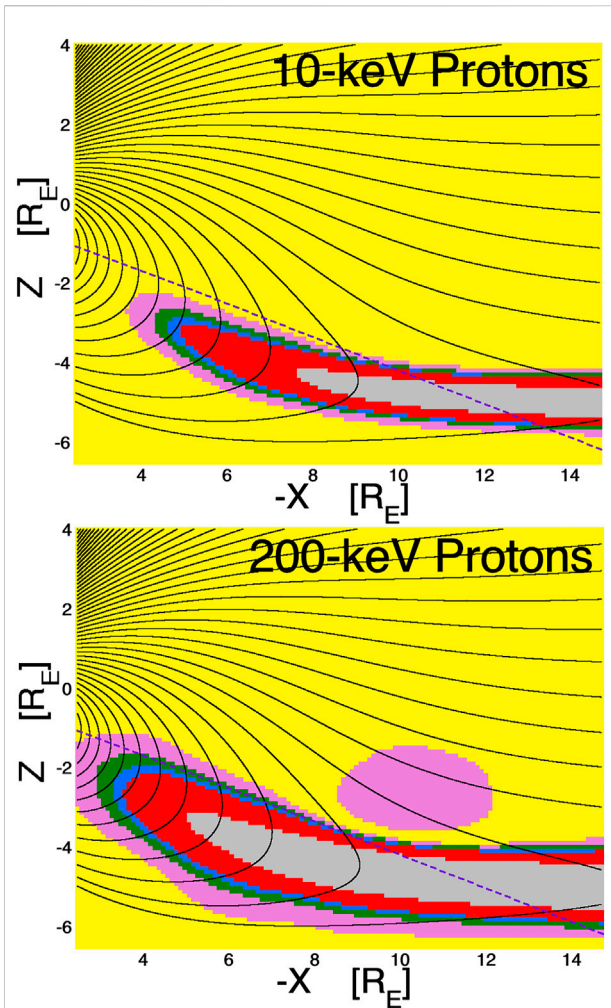


**FIGURE 4**  
 Loss-cone-shift maps for protons. Magnetic-field lines in the nightside magnetosphere in the noon-midnight meridian are drawn as the black curves using the T96 magnetic-field model. The colored shading is the calculated eastward shift of the local atmospheric loss cone for 10-keV protons (top panel) and for 100-keV protons (bottom panels) based on the T96 magnetic-field model. The color scheme is yellow (shift  $<0.5^\circ$ ), pink (shift  $0.5^\circ-1^\circ$ ), green (shift  $1^\circ-1.5^\circ$ ), blue (shift  $1.5^\circ-2^\circ$ ), red (shift  $2^\circ-10^\circ$ ), and gray (shift  $>10^\circ$ ).

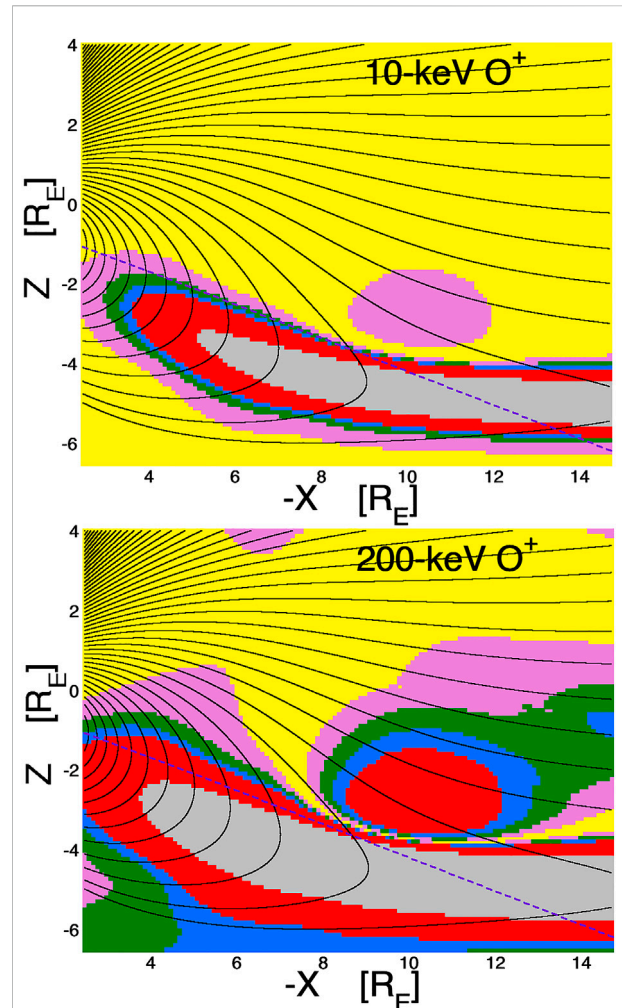


**FIGURE 5**  
 Loss-cone-shift maps for oxygen  $O^+$ . Magnetic-field lines in the nightside magnetosphere in the noon-midnight meridian are drawn as the black curves using the T96 magnetic-field model. The colored shading is the calculated westward angular shift of the local atmospheric loss cone for 10-keV  $O^+$  (top panel) and for 200-keV  $O^+$  (bottom panels) based on the T96 magnetic-field model. The color scheme is yellow (shift  $<0.5^\circ$ ), pink (shift  $0.5^\circ-1^\circ$ ), green (shift  $1^\circ-1.5^\circ$ ), blue (shift  $1.5^\circ-2^\circ$ ), red (shift  $2^\circ-10^\circ$ ), and gray (shift  $>10^\circ$ ).

oxygen than for protons. The maps of Figure 5 indicate that the angular shift of the loss cone can be significant ( $\theta_{\text{shift}} > 2^\circ$ , red shading) for 200-keV  $O^+$  at  $L = 2.5$  and the loss cone shift can be significant for 10-keV  $O^+$  at  $L = 4$ . The gray shading ( $\theta_{\text{shift}} > 10^\circ$ ) in the two panels of Figure 5 indicates that one can expect 10-keV  $O^+$  to have stochastic orbits at  $L = 5$  and 200-keV  $O^+$  to have stochastic orbits at  $L = 4$  owing to field-line-curvature scattering.

Using the T96 model for  $B_z = -5$  nT and  $Dst = -30$  nT with no dipole tilt, four loss-cone-shift maps in the equatorial plane of the magnetosphere are plotted in

Figure 6. The upper-left panel is the magnitude of the eastward shift for 1-MeV electrons, the upper-right panel is the westward shift for plasma-sheet-energy (10-keV) protons, the lower-left panel is the westward shift for substorm-injection-energy (100-keV) protons, and the lower-right panel is the westward shift for plasma-sheet-energy (10-keV)  $O^+$  ions. In each panel the Sun is off to the left and the magnetotail is on the right. The yellow shading in each panel represents equatorial regions where the loss-cone shift is minor ( $<5^\circ$ ). For the 1-MeV electrons the inner magnetosphere ( $<5 R_E$ ) exhibits minor shifts, but moving

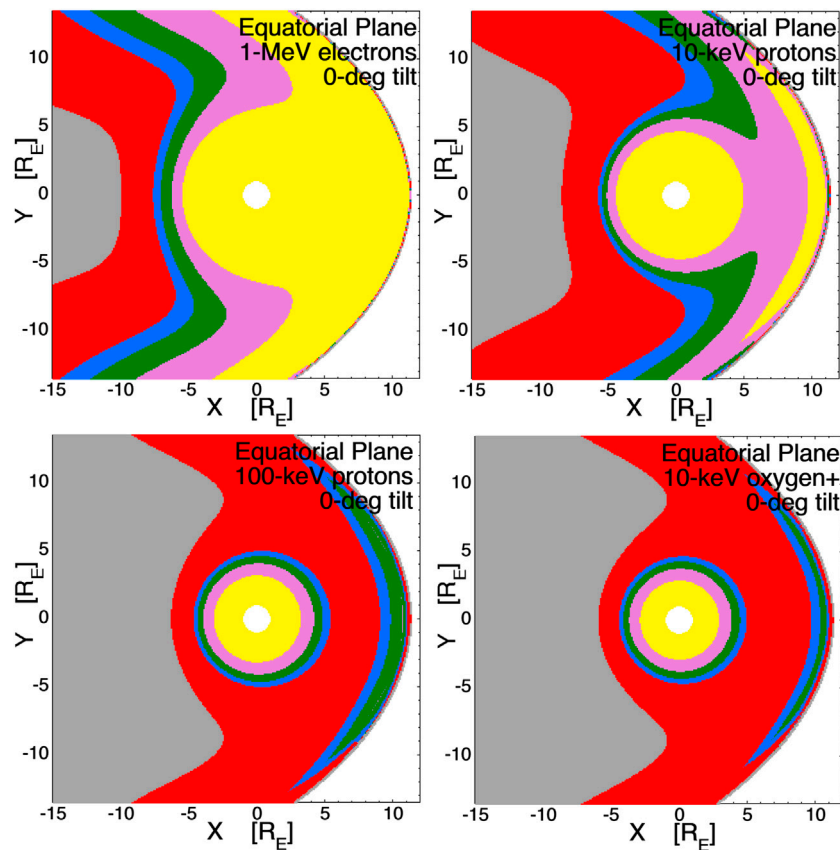


**FIGURE 6**

Loss-cone-shift maps in the equatorial plane using the T96 magnetic-field model with no dipole tilt. The upper-left is for 1-MeV electrons, the upper right is for 10-keV protons, the lower-left is for 200-keV protons, and the lower-right is for 10-keV oxygen  $O^+$ . The color scheme is yellow (shift  $< 0.5^\circ$ ), pink (shift  $0.5^\circ - 1^\circ$ ), green (shift  $1^\circ - 1.5^\circ$ ), blue (shift  $1.5^\circ - 2^\circ$ ), red (shift  $2^\circ - 10^\circ$ ), and gray (shift  $> 10^\circ$ ).

into the transition region and the magnetotail the shift becomes serious. For all four panels of Figure 6 recall that stochastic (finite-larmor-radius) scattering comes in strongly when the loss-cone shift exceeds about  $5^\circ$ , so the red-shaded region marks the transition to stochastic scattering and the gray shaded regions are fully stochastic. For the 10-keV protons (upper-right) the magnitudes of the loss cone shifts are everywhere more serious than they are for the energetic electrons. Even at geosynchronous orbit ( $6.6 R_E$ ) the shift is serious and stochastic behavior is probably present across the nightside. For the energetic protons and the 10-keV oxygen (bottom two panels) only the very inner magnetosphere would exhibit mild loss-cone shifts and geosynchronous orbit ( $6.6 R_E$ ) would be populated with stochastic orbits. The lower-left panel indicates that what would be commonly called “ring-current” protons at 100-keV may be stochastically scattering in the regions inward of geosynchronous orbit where researchers label the hot ions as ring-current ions.

## Discussion

A conclusion of the examination of the loss-cone-shift maps is that the angular shift of the loss cone can be important for energetic ions, and even thermal (plasma-sheet) ions throughout the middle and outer magnetosphere and certainly in the magnetotail. Another conclusion is that stochastic scattering *via* field-line curvature can be important for hot and energetic ions, even in the dipolar portions of the magnetosphere. Hence, ring-current protons and oxygen ions are probably undergoing stochastic scattering. For electrons, important loss-cone shifts and stochastic scattering are limited to the stretched portion of the magnetotail near and beyond the transition region.

Example maps of the magnitude of the loss cone shift for electrons, protons, and oxygen  $O^+$  ions were created using the T96 (Tsyganenko, 1995; Tsyganenko and Stern, 1996) magnetic-field model with the input parameters  $B_z = -5$  nT for the solar wind and  $Dst = -30$  nT. In the interest of compactness, no parameter variations were performed and no other magnetic-

field models were explored. Different magnetic-field models were briefly explored in Sect. 5 of Borovsky et al., 2022b and the different models produce different shift magnitudes (cf. Fig. 9 of Borovsky et al., 2022b).

For future exploration of parameters, the author has a simple-to-use (relativistic) FORTRAN code to efficiently calculate the loss cone shifts for various particle types. The author will make that code available upon request.

## Data availability statement

The original contributions presented in the study are included in the article/Supplementary Material; further inquiries can be directed to the corresponding author.

## Author contributions

JB initiated this project, performed the numerical orbit calculations, and wrote the manuscript.

## Funding

JB was supported at the Space Science Institute by the NSF GEM Program via grant AGS-2027569, by the NASA HERMES

Interdisciplinary Science Program via grant 80NSSC21K1406, and by the NASA Heliophysics Mission Concept Studies Program via award 80NSSC22K0113.

## Acknowledgments

The author thanks Gian Luca Delzanno and Kateryna Yakymenko for helpful conversations.

## Conflict of interest

The authors declare that the research was conducted in the absence of any commercial or financial relationships that could be construed as a potential conflict of interest.

## Publisher's note

All claims expressed in this article are solely those of the authors and do not necessarily represent those of their affiliated organizations, or those of the publisher, the editors and the reviewers. Any product that may be evaluated in this article, or claim that may be made by its manufacturer, is not guaranteed or endorsed by the publisher.

## References

- Birmingham, T. J. (1984). Pitch angle diffusion in the Jovian magnetodisc. *J. Geophys. Res.* 89, 2699–2707. doi:10.1029/ja089ia05p02699
- Borovsky, J. E., Delzanno, G. L., Dors, E. E., Thomsen, M. F., Sanchez, E. R., Henderson, M. G., et al. (2020a). Solving the auroral-arc-generator question by using an electron beam to unambiguously connect critical magnetospheric measurements to auroral images. *J. Atmos. Sol. Terr. Phys.* 206, 105310. doi:10.1016/j.jastp.2020.105310
- Borovsky, J. E., Delzanno, G. L., and Henderson, M. G. (2020b). A mission concept to determine the magnetospheric causes of aurora. *Front. Astron. Space Sci.* 7, 595292. doi:10.3389/fspas.2020.595292
- Borovsky, J. E., Delzanno, G. L., and Yakymenko, K. N. (2022a). Pitch-angle diffusion in the Earth's magnetosphere organized by the Mozer-transformed coordinate system. *Front. Astron. Space Sci.* 9, 810792. doi:10.3389/fspas.2022.810792
- Borovsky, J. E., Yakymenko, K. N., and Delzanno, G. L. (2022b). Modification of the loss cone for energetic particles in the Earth's inner magnetosphere. *J. Geophys. Res.* 123, e2021JA030106. doi:10.1029/2021JA030106
- Chirikov, B. V. (1987). Particle confinement and adiabatic invariance. *Proc. Roy. Soc. Lond. A* 413, 145–156.
- Il'in, V. D., Kuznetsov, S. N., Yushkov, B. Y., and Il'in, I. V. (1992). Quasiadiabatic model of charged-particle motion in a dipole magnetic confinement system under conditions of dynamic chaos. *JETP Lett.* 55, 645–649.
- Il'ina, N., Il'in, V. D., Kuznetsov, S. N., Yushkov, B. Y., Amirkhanov, I. V., and Il'in, I. V. (1993). Model of nonadiabatic charged particle motion in the field of a magnetic dipoles. *JETP* 77, 246–252.
- Mozer, F. S. (1966). Proton trajectories in the radiation belts. *J. Geophys. Res.* 71, 2701–2708. doi:10.1029/jz071i011p02701
- Porazik, P., Johnson, J. R., Kaganovich, I., and Sanchez, E. (2014). Modification of the loss cone for energetic particles. *Geophys. Res. Lett.* 41, 8107–8113. doi:10.1002/2014gl061869
- Powis, A. T., Porazik, P., Greklek-McKeon, M., Amin, K., Shaw, D., Kaganovich, I. D., et al. (2019). Evolution of a relativistic electron beam for tracing magnetospheric field lines. *Front. Astron. Space Sci.* 6, 69. doi:10.3389/fspas.2019.00069
- Roederer, J. G., and Zhang, H. (2014). *Dynamics of magnetically trapped particles*. Berlin: Springer-Verlag.
- Sanchez, E. R., Powis, A. T., Kaganovich, I. D., Marshall, R., Porazik, P., Johnson, J., et al. (2019). Relativistic particle beams as a resource to solve outstanding problems in Space Physics. *Front. Astron. Space Sci.* 6, 71. doi:10.3389/fspas.2019.00071
- Tsyganenko, N. A. (1995). Modeling the Earth's magnetospheric magnetic field confined within a realistic magnetopause. *J. Geophys. Res.* 100, 5599. doi:10.1029/94ja03193
- Tsyganenko, N. A., and Stern, D. P. (1996). Modeling the global magnetic field of the large-scale Birkeland current systems. *J. Geophys. Res.* 101, 27187–27198. doi:10.1029/96ja02735
- Willard, J. M., Johnson, J. R., Snelling, J. M., Powis, A. T., Kaganovich, I. D., and Sanchez, E. R. (2019). Effect of field-line curvature on the ionospheric accessibility of relativistic electron beam experiments. *Front. Astron. Space Sci.* 6, 56. doi:10.3389/fspas.2019.00056